Phase separation in alumina-rich glasses to increase glass reactivity for low-CO_2 alkali-activated cements

P. Kinnunen[a,b,*], H. Sreenivasan[a], C. R. Cheeseman[b], and M. Illikainen[a]

[a.] *Fibre and Particle Engineering Research Unit, University of Oulu, Finland*
[b.] *Department of Civil and Environmental Engineering, Imperial College London, London SW7 2BU, United Kingdom*
[*] *Corresponding author paivo.kinnunen(at)oulu.fi*

Keywords: Alkali Activated Cement, Glass, Supplementary Cementitious Material

Abstract

Ways to reduce cement-related carbon emissions are actively sought. One possible solution is partial substitution of Portland cement by alkali-reactive glass. We report on low-CO_2 glass compositions that have high alkali solubility derived from industrial basaltic stone wool compositions. We found that highly alkali-soluble glasses can be formed with glass compositions that in principle can be made using silicate minerals which have no raw material-related CO_2 emissions. The reason behind the reactivity of these glasses is thought to be caused by the dilution of the main network-forming species, silicon, which is further enhanced by phase separation, forming phases with high-silicon and low-silicon concentrations. Phase separation in alumina-rich samples is further studied and occurs at moderate cooling rates. The effect of glass-glass phase separation is discussed in the context of reactive glasses in cementitious systems. The results indicate that controlled phase separation could decouple CO_2 emissions from the reactivity of glassy supplementary cementitious materials.

1. Introduction

According to a 2016 UNEP report, the Portland cement industry is responsible for 6-8% of the annual anthropogenic CO_2 emissions and this is constantly increasing (Scrivener et al., 2016). Roughly half of these 1 435 Mt/a emissions originate from energy used in processing cement, while the other half is “unavoidable” in the sense that it is inherent in the binder chemistry; it is a by-product of producing CaO from $CaCO_3$ (Intergovernmental Panel on Climate Change and Edenhofer, 2014).

To lower CO_2 emissions of Portland cement, supplementary cementitious materials (SCM) are used extensively, most notably calcined clays, glassy waste materials and finely ground calcium carbonate. Another approach to lower the cement-related CO_2 emissions is the development of alternative cements, such as alkali activated cements (AAC). Alkali activated cements consist of an alkali-soluble alumina-silicate source that is reacted with an alkali, most often sodium silicate, which then hardens into concrete but with up to 78% lower CO_2 emissions (Habert and Ouellet-Plamondon, 2016) . Both of these approaches are used to valorize glassy industrial side streams, such as metallurgical slags and coal power fly ash. However, due to the low and declining amount of these industrial wastes compared to cement manufacturing volumes, there is a growing need for synthetic low-CO_2 glasses that could be used to supplement cement in order to reduce cement CO_2 emissions to zero or below by 2050 as required by climate predictions.

Reactivity of a glass depends largely on its chemical composition. The oxide of silicon (SiO_2) is an excellent glass former, and produces a strong covalently bonded silicon network linked by bridging oxygen (BO) atoms. Modifying ions (alkali or alkali earth metals) enter the glass network as singly or doubly charged cations and occupy interstitial sites while remaining weakly bonded (**Figure 1**) (Henderson, 2005; Mysen and Richet, 2005; Newlands et al., 2017). Charge compensation is achieved by the creation of "non-bridging" oxygen atoms (NBO) that lead to an increased disruption (de-polymerization) of the base silica network (Greaves and Sen, 2007). The creation of NBOs therefore reduces the connectivity of the glass network and this increases alkaline reactivity (Mills et al., 2011). Therefore reactivity can be approximated by a single number: the amount of non-bridging oxygen atoms per network former (NBO/T) (Li et al., 2010; Mills et al., 2011; Perchuk and Kushiro, 2013, p. 152; Schöler et al., 2017).

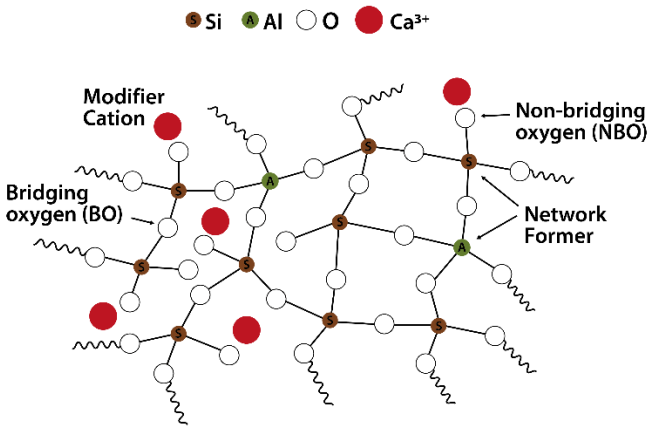

Figure 1: *Local structure of simplified CaO-Al_2O_3-SiO_2 glass highlighting the bridging (BO) and non-bridging oxygen atoms (NBO). Figure adapted from (Newlands et al. 2017).*

The most common minerals in the Earth's crust have relatively low NBO/T-ratio due to their high Si content. A widely used method to increase glass (or slag) reactivity is to add CaO which disrupts the silicon network, and increases the NBO/T and with it, reactivity. While effective, this CaO addition as an industrial practice comes with increased CO_2 emissions. Calcium is found mainly as $CaCO_3$ and CaO is derived through the de-carbonation reaction: $CaCO_3 \rightarrow CaO + CO_2$. Therefore, there is often a trade-off between reactivity and CO_2 emissions of glasses (Moesgaard et al., 2012; Oey et al., 2017; Schöler et al., 2017; Snellings, 2013).

For example, Moesgaard et al. (2010) developed a CaO-Al_2O_3-SiO_2 glass that contains 22% of $CaCO_3$-derived calcium, and which can be used to replace 30% OPC in concrete. Here, we take a different approach, where the ultimate aim is to find a reactive glass composition that could be manufactured without chemical carbon dioxide emissions, and that could be then alkali-activated using $NaOH/Na_2CO_3$ solutions (Ke et al., 2016). The chemical CO_2 emissions will be referred to as RM-CO_2 here, and only account for the "unavoidable" emissions related to the decarbonation of minerals such as $CaCO_3$. Alternative calcium sources are silicate minerals, such as basalt and gabbro. These minerals have a complex chemical composition, which renders them unsuitable raw materials for most industrial glasses, where optical clarity is required, whereas industrial glasses for SCM's have no requirements to optical clarity, thus basalt and gabbro can be used. Basalt is regularly used as a raw material for stone wool. The compositions chosen for this study can in principle be formed from silicate minerals, although here we have prepared them using a pure model system based on carbonates to ensure purity. Since the alkali activator in AAC (often NaOH or Na_2CO_3) can be derived from seawater with negligible RM-CO_2 emissions (U.S. Environmental Protection Agency, 1992), this alkali-activated glass cement would theoretically have no RM-CO_2 emissions. Other CO_2 emissions can be estimated by the energy-intensity, which will be done in a later section.

Recently, stone wool has been found to be highly reactive both in alkali activated cements, as well as SCM applications (Cheng et al., 2011; Kinnunen et al., 2017; Lin et al., 2012; Yliniemi et al., 2016). Stone wool is made by melting and fiberizing basaltic glass, which has relatively low CaO content (20%). The reactivity of these glasses originates partially from the high-energy state of the glass, arrived at by hyper-quenching in which fibres are cooled at 10^6 K/s, which preserves iron in the ferrous state (Moesgaard et al., 2011, 2007; Yue et al., 2004). However, such

cooling rates are not amenable to highly-efficient manufacturing of cementitious materials, where cooling rates of 10^1 K/s are used (Barati et al., 2011; Qin et al., 2015).

Therefore, the goal of this work was to assess if such basaltic multicomponent glasses with near-zero RM-CO_2 emissions could be made with low cooling rates (10 K/s), and whether they have potential as an alkali activated cement precursor. The results are discussed within the context of the utilization potential in activated cements and as manufactured SCM and the reactivity is compared to other glassy materials used in cements.

2. Materials and Methods

The raw materials used for the glass synthesis included fumed silica (SiO_2, Sigma), aluminum oxide (Al_2O_3, Sigma-Aldrich), calcium carbonate ($CaCO_3$, VWR Chemicals), magnesium carbonate ($MgCO_3$, Acros Organics), ferric oxide (Fe_2O_3, Merck), sodium carbonate ($NaCO_3$, Sigma), and titanium (IV) oxide in anatase form (TiO_2, Aldrich). For glass solubility experiments, sodium hydroxide (NaOH) with a purity >99% (Merck), and nitric acid (HNO_3, Sigma-Aldrich) were used. Deionized water was used whenever necessary. Metakaolin used as a reference was commercial "High quality pozzolanic cement additive" from BASF ($Al_2O_3 \cdot 2SiO_2$, MetaMax®).

Six artificial glass samples were prepared with wt.% compositions according to equation $(60 - X)SiO_2 \cdot XAl_2O_3 \cdot 18CaO \cdot 10MgO \cdot 5Fe_2O_3 \cdot 5Na_2O \cdot 1.5TiO_2$, where X was varied from 11 to 21. The compositions were designed to partly fall into the biosoluble range used in stone wool manufacturing (C5 and C6), and C1-C4 are aluminum-poor (Guldberg et al., 2002). The raw materials were mixed in appropriate proportions and ground in a vibratory disc mill (Retsch RS 200) at 1000 rpm for 60 seconds. The mixes were then melted in a corundum (Al_2O_3) crucible (40 g batch size) inside in a Nabertherm high temperature furnace (HT 08/18) in air in two stages: first at 1050°C for 120 min to remove carbon originating from the carbonate raw materials and then at 1600°C for 120 min to produce the melt. A heating rate of 20°C/min was used in both cases. The melt obtained after the second stage was quenched by pouring it onto a water-cooled copper plate to obtain glass. All the glass samples were finely ground in the vibratory disc mill (1-5 min, 1000 rpm) to obtain an average particle size between 1 µm and 10 µm before being used for further experiments.

Diffraction patterns of the glass samples were recorded using a Rigaku SmartLab 9 kW XRD machine. For the purpose of analysis, Co Kα radiation (Kα1=1.78892 Å; Kα2=1.79278 Å; Kα1/Kα2=0.5), and scan rate of 3°/min between 5°and 85° (2θ) with 0.02°/step were used. The elemental concentration in liquid samples from the glass solubility test was determined using a Thermo Fisher Scientific iCAP6500 Duo inductively coupled plasma optical emission spectrometer (ICP-OES) fitted with a Cetac ASX-520 auto sampler. Scanning transmission electron microscopic (STEM) images of C6 glass sample was obtained using a LEO 912 OMEGA EFTEM fitted with energy-dispersive X-ray spectroscopy (EDS) detector.

All the synthetic glass samples prepared were analyzed for alkaline solubility. During the solubility test, finely ground glass samples was mixed with 6 M NaOH solution in closed polypropylene containers using a liquid to solid ratio of 40 w/w. The test was performed under shaking condition (Mot = 150/min) using a horizontal shaking table (IKA KS 260 orbital shaker) at 23 ± 0.5°C for 24 h. After the solubility test, all samples were filtered using a 0.45 μm polypropylene filter paper. The filtrate was acidified with 6 M HNO_3 to pH less than 2 and was analyzed using ICP-OES to determine the soluble elemental concentrations. The solid residue was washed with deionized water and finally dried inside a desiccator for 48 hours. The dried solid residue was finally characterized by XRD and STEM.

Initial rate of dissolution experiments were completed also in 6 M NaOH solution using a 400 w/w liquid-solid ratio to prevent secondary product formation. The experiment was performed in stationary condition at room temperature in polypropylene bottle (sample volume being 350 ml) and 5 ml samples were periodically taken for elemental analysis. Sampled liquid was filtered with 0.45 μm polypropylene filter paper (treatment of filtrate was similar to previous solubility test), and analyzed with ICP-OES. Surface area of the glass was analyzed by with the help of Micrometrics ASAP2020 (4.162 m^2/g for C6 and 11.650 m^2/g for metakaolin).

3. Results and Discussion

Six batches of artificial glass were prepared to fall partly within the biosoluble range given for high-aluminum stone wool (the range has been appointed CAS registry number 287922-11-6) (Guldberg et al., 2002). Aluminum is critical in biosolubility (Devreux et al., 2010), and therefore aluminum content was varied according to the equation $(60 - X)SiO_2 \cdot XAl_2O_3 \cdot 18CaO \cdot$

$10MgO \cdot 5Fe_2O_3 \cdot 5Na_2O \cdot 1.5TiO_2$, where X was varied from 11 to 21 (**Table 1**). The CAS range is designed to guarantee sufficient biosolubility in MMVF applications (Guldberg et al., 2002). However the implications to high pH solubility of this 8-component compositional range have not been studied previously. A distinction between biosolubility and alkali-solubility needs to be made: biosolubility is defined by the dissolution rate of the material at physiological pH (around pH 4-5) in the presence of organic complexing agents (Guldberg et al., 2002). Alkali-solubility refers here to the pH range that is relevant to activated cements (pH 13-15), where glass dissolution proceeds via a different mechanism, and the dissolution rates between high and low pH are not necessarily correlated. Indeed stone wool is known to be more amenable to leaching in acidic than alkaline conditions. Therefore, the alkali solubility in 24-hours was measured for all glasses, and the most soluble sample (C6) subjected to more detailed analysis.

Table 1: Target compositions of the prepared glasses expressed in wt%.

	SiO_2	Al_2O_3	CaO	MgO	Na_2O	TiO_2	Fe_xO_y
C1	49	11	18	10	5	1.5	5
C2	47	13	18	10	5	1.5	5
C3	45	15	18	10	5	1.5	5
C4	43	17	18	10	5	1.5	5
C5	41	19	18	10	5	1.5	5
C6	39	21	18	10	5	1.5	5

All glasses were X-ray amorphous, as evidenced by the absence of Bragg peaks in the XRD pattern in**Figure 2 Figure 2**. This result is in itself important, since the cooling rate used (13 K/s) was five orders of magnitude lower than used in industrial stone wool synthesis (10^6 K/s). The absence of long-range structural order in the material is important, because crystalline phases would render the material unreactive in cement synthesis (Juenger et al., 2012).

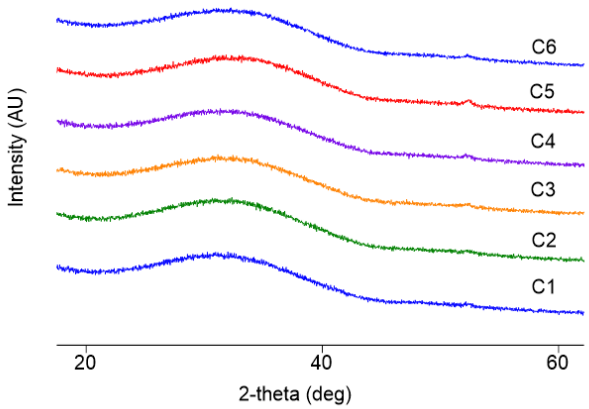

***Figure 2**: X-ray diffraction patterns for the prepared glasses, showing their X-ray amorphous nature.*

All glasses possessed excellent alkali reactivity, estimated by measuring the leached fraction after 24 h in 6 M NaOH and compared to metakaolin as a highly-reactive reference material. The reactivity of the glasses was assessed by 24-hour dissolution experiment, in 6 M NaOH solution, using two indicator cations, silicon and aluminum. The leached fraction after 24-hour dissolution was defined for the indicator cations (i = Si, Al) as the ratio of the dissolved mass (m_i^d) to the mass in the original glass (m_i^g):

$$LF_i = \frac{m_i^d}{m_i^g} \cdot 100 = \frac{C_i V}{f_i \mathrm{m}} \cdot 100 \qquad (1)$$

where m is the mass of the glass powder before corrosion, C_i is the concentration of the studied element (mg/ml), V is the sample volume (ml), f_i the elemental fraction in the glass (mg/g) and m is the starting mass of the glass (g). All glasses possess alkali reactivities considerably higher than the reference (see **Figure 3a**). In a previous study, Panagiotopoulou *et al.* (2007) found metakaolin to be the most reactive of the studied materials in 10 M NaOH. The overall reactivity increased with increasing aluminum content in the glass, and the dissolution of aluminum was preferential to silicon in all glasses. The preferential dissolution of aluminum could be explained by precipitation of secondary phases, such as amorphous silica. However amorphous silica is not visible in XRD, and it could not therefore be confirmed. Mg and Al were found to precipitate as meixnerite-type hydrotalcite ($Mg_6Al_2(OH)_{18}$•$4(H_2O)$), and some carbonation was observed in the form of calcite ($CaCO_3$), see **Figure 3b**. Therefore, even though the reactivity assessment underestimated the reactivity, all glasses were found to possess higher alkali-reactivity than metakaolin. This was true regardless of the indicator element.

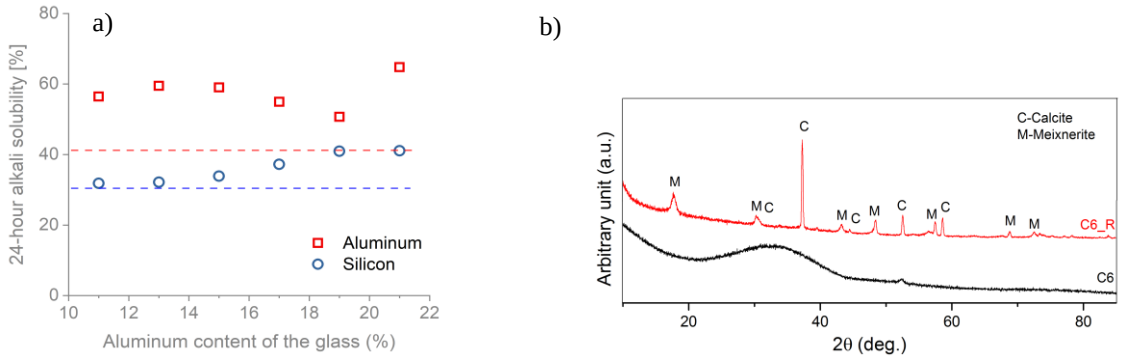

***Figure 3**: Reactivity of the prepared glasses. a) 24-hour alkali solubility using aluminum and silicon as indicator cations. Dashed lines are the solubility of metakaolin as a reference under the same conditions. The solubilities of iron, calcium and magnesium were below 1%, which suggest there is precipitation during the test. b) XRD of leftover for C6 glass compared to the starting material, showing the precipitation of calcite and meixnerite-type hydrotalcite.*

The 24-hour reactivity test gives a rough measure of reactivity, but does not allow for accurate comparison between materials. Fineness of the material directly affects the results, as dissolution rate and therefore reactivity is linearly dependent on the available glass surface area. Therefore the most reactive glass, C6, was submitted to the initial rate of dissolution analysis, along with metakaolin.

The reactivity of C6 was further evaluated by the initial dissolution rate. A more accurate measure of the reactivity of glass can be determined by measuring initial dissolution rate (k_i^+) under relevant pH conditions (Devreux et al., 2010; Hamilton et al., 2001). Dissolution was measured at pH 14,8 (6 M NaOH), and the initial rate was calculated using silicon and aluminum as indicator cations using the following equation:

$$k_i^+ = \frac{V}{Sf_i}\frac{\mathrm{d}C_i}{\mathrm{d}t}\Big|_{t=0} \qquad (2)$$

where k_i^+ is the initial rate of dissolution of the glass calculated using indicator cation i, V is sample volume (L), S is the surface area of the material exposed to the solution (m^2), C_i is the measured elemental concentration in solution (moles/L), and t elapsed time (s).

Indicator cation concentrations were below saturation levels of secondary precipitates, and a plateau was reached after 24 hours for C6 and at 48 hours for metakaolin (**Figure 4a**). When the lower fraction of indicator elements in the glass was taken into account, the reacted fraction of C6 was similar to metakaolin (**Figure 4b**). However, due to the differences in available surface area (11.65 m^2/g and 4.16 m^2/g for metakaolin and C6 respectively) the initial dissolution rate of C6 was considerably higher than metakaolin (**Figure 4c**). Indeed, the rate of dissolution is much higher in the test conditions than is usual for SCM's in Portland cement systems. $CaO\text{-}Al_2O_3\text{-}SiO_2$glasses from a range of industrially relevant SCM's with varying amounts of Ca in pH 13 (relevant to Portland cement), as studied by Snellings (Snellings, 2013), is shown as a point of comparison (**Figure 4c**). This is not direct comparison due to the different pH conditions (except in the case of C6 and metakaolin) and the results are applicable only in alkali activated systems.

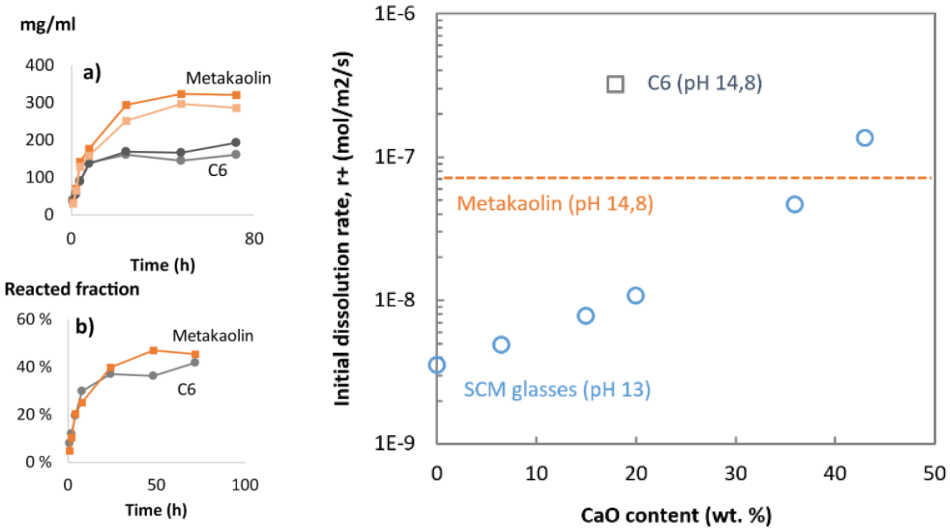

Figure 4: a) Measured concentrations as a function of time for metakaolin and C6 in 6M NaOH as measured by using Al and Si as the indicator element (Al in darker color). b) Calculated reacted fraction based on total dissolved silicon. c) Initial dissolution rate calculated based on dissolved aluminum in the initial linear phase. Comparison data for SCM from Snellings 2013.

Understanding glass dissolution through local glass structure and NBO/T. Glass consists of network formers and network modifiers. The former are four-coordinated elements forming the network of the glass, and the latter are highly coordinated and bound via ionic bonds. Therefore, network modifier-rich glasses are naturally more alkali soluble. In the current system Si

is the main network former; Ca, Na and K are network modifiers while Al and Fe are so-called intermediates that can have both roles (Waychunas et al., 1988).

In slag utilization and supplementary cementitious material (SCM) glasses, NBO/T is often used to predict alkali reactivity (NBO/T: non-bridging oxygen per tetrahedral cation) (Durdziński et al., 2015; Tiwary et al., 2013). In complex multicomponent systems such as slag and basalt glasses the calculation of NBO/T is not straightforward and several assumptions have to be made. Most notably, it is assumed that both Al and Fe can be network formers and network modifiers. In this case, NBO/T can be calculated by inserting the oxide fractions into the following equation:

$$\frac{NBO}{T} = \sum_{i=1}^{i} n\, M_i^{n+}/T \qquad (3)$$

where M'* represent network-modifying cations. The sum is obtained after subtraction of the proportion of metal cations necessary for charge-balance of Al^{3+} and Fe^{3+} (Mysen et al., 1985, 1982). Therefore, NBO/T was calculated using equation 4:

$$\frac{NBO}{T} = \frac{2\left(X_{CaO}+X_{MgO}+3f_{Fe}X_{Fe_2O_3}+3f_{Al}X_{Al_2O_3}+X_{Na_2O}+X_{K_2O}-(1-f_{Al})X_{Al_2O_3}-(1-f_{Fe})X_{Fe_2O_3}\right)}{X_{SiO_2}+2(1-f_{Al})X_{Al_2O_3}+2(1-f_{Fe})X_{Fe_2O_3}+X_{TiO_2}}, \qquad (4)$$

where f_{Al} and f_{Fe} are the fraction of aluminum and iron in network modifier role.

Structural information is needed in order to assign the network-forming cations (T-cations). According to solid state NMR data, aluminum is in tetrahedral coordination in silicate melts if metal cations M^{2+} or M^{+} are present in sufficient quantities to charge-compensate $(AlO_4)^{5-}$ tetrahedra as $M_{0,5}^{2+}(AlO_4)^{4-}$ or $M_1^{+}(AlO_4)^{4-}$ complexes (Lee and Stebbins, 2000; Merzbacher et al., 1990; Mysen et al., 1985, 1982; Neuville et al., 2006). The molar ratio $(Fe^{3+} + Al^{3+})/(0.5M^{2+} + M^{+})$ is a measure of this quantity, and based on the chemical composition of the prepared glasses the ratio varies between 0.35 and 0.59, well below 1 (**Table 2**). Malfait *et al*. (2012) studied the local structure of less charge-balanced complex glass (andesite composition) using ^{27}Al NMR spectroscopy and found that 98% of aluminum was four-coordinated. The corresponding value for f_{Al} (0,02) was therefore assumed here as well. Since glasses were prepared in oxidizing conditions, Fe can assumed to be in an oxidized Fe^{3+}

state, which is also largely in tetrahedral coordination with the same charge-balancing constraints as for Al^{3+} (Mysen et al., 1985). Therefore f_{Fe} was also set 0,02 in equation 4.

Using these values ($f_{Al} = f_{Fe} = 0{,}02$), equation 4 gives NBO/T below unity, and decreasing with increasing aluminum content (**Table 2**). Therefore, NBO/T alone cannot be used to explain the high initial dissolution rate of glass C6 and increasing leached fraction with increasing Al content (**Figure 3a**). The NBO/T calculations are approximate due to the lack of structural information as well as actual sample oxide compositions. Especially Al_2O_3 content might be slightly affected by possible contamination from the corundum crucibles.

Table 2: *Structural characteristics of the glasses based on molar ratios.*

	C1	***C2***	***C3***	***C4***	***C5***	***C6***
$(Fe^{3+} + Al^{3+})/(0.5M^{2+} + M^{+})$	0,35	0,40	0,44	0,49	0,54	0,59
NBO/T	0,94	0,91	0,87	0,83	0,80	0,76

Earlier studies have found that glass dissolution rates decrease with increasing SiO_2 content (Jantzen and Plodinec, 1984; Perret et al., 2003; Wolff-Boenisch et al., 2004). Wolff-Boenish *et al.* (2004) studied the dissolution rate dependence on SiO_2 content and found the dissolution rate in volcanic glasses is exponentially related to SiO_2 content between 46% and 73%. The relationship was more clear under acid (pH 4) than alkali (pH 10,6) conditions. The high dissolution rate of C6 could therefore be partially explained by the dilution of SiO_2 in the multicomponent system, where the presence of MgO, Fe_2O_3 and TiO_2 in addition to CaO, Na_2O and Al_2O_3 decreases Si content and therefore increases dissolution rate. The reactivity is not directly increased by lowering the SiO_2 amount in this study (**Figure 3a**), and therefore the dilution of SiO_2 alone cannot explain the high rates of dissolution.

Phase separation. Another factor associated with high leaching rates at higher aluminum content in the synthetic glasses could be phase separation. The role of phase separation in the preparation of reactive AAC glasses and SCMs has not been extensively investigated, and is sometimes disregarded in glass preparation protocols. However, phase separation is a well-

controlled phenomenon, and it has been found to increase the reactivity of blast furnace slag in cements (Li et al., 2009), as well as glass reactivity in glass-ionomer cement systems (Hill and Wilson, 1988).

To investigate the presence of phase separation, the most and least reactive glasses (C1 and C6) were subjected to transmission electron microscopy (TEM) analysis. TEM images show phase separation in glass C6 (**Figure 5**), which was not present in the lower Al content C1 (Supplementary information). EDX mapping of the TEM images also revealed that 1) MgO was depleted in all glasses compared to the target compositions, 2) C1 composition was close to the target composition, fully consistent with homogenous non-phase-separated glass, and 3) phase separated glass (C6) consisted of silicon-rich and modifier-rich regions. Furthermore, in C6 the target composition could be arrived at arithmetically by assuming 22% volume contribution from the silicon-rich and 78% volume contribution from the modifier-rich glass (R^2 of 0,92).

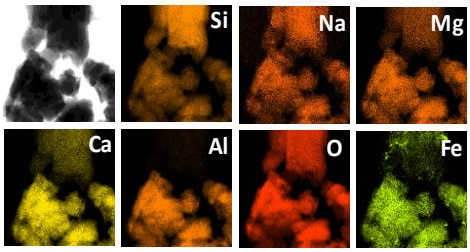

Figure 5: *phase separation in C6 evidenced by the TEM observation. In the EDX maps silicon can be seen to have concentrated to the particle visible on the top of the figure, sodium and oxygen are somewhat equally distributed, while magnesium, calcium, iron, and especially aluminium are concentrated to the particles at the bottom.*

Phase separation in the quenched melt can originate from liquid-liquid phase separation above the melting temperature, or it can result from a nucleation process during cooling. Regardless, the presence of Mg and Fe increases the tendency to form separated phases (Karamanov et al., 2000; Mysen et al., 1982). Melts tend to become more prone to phase separation as NBO/T reduces below 1 in the simplified glass system CaO-MgO-SiO_2, and this intensifies when the fraction of MgO increases (Mysen et al., 1982). Similarly, iron-containing glasses are characterized by a tendency to undergo liquid immiscibility (Karamanov et al., 2000). Glasses with a similar composition (wt%: 44.6 SiO_2, 18.1 Al_2O_3, 2.1 TiO_2, 8.0 FeO, 13.0 CaO, 9.8 MgO, 2.4 K_2O, 1.0 Na_2O) have been found to show phase separation when held at temperatures below their melting point. They only crystallized if kept at elevated temperatures (Moesgaard et al., 2007). Similar behavior is suspected

therefore to have happened in glass C6. This was supported by melt simulations (data not shown) that found a non-separated liquid phase at 1600 °C and 1 Atm pressure (simulations done with FactSage thermochemical software).

Hrubÿ parameter. In melt compositions that are prone to phase separation, separation can occur during cooling if the cooling rate is low enough to initiate nucleation but high enough to prevent crystallization. Therefore to investigate this possibility, the *Hrubÿ parameter* was calculated for the glasses. The Hrubÿ parameter is an empirical parameter used to estimate glass forming ability or the minimum rate of cooling that is required to avoid crystallization, the *critical cooling rate* (Cabral et al., 1997). The Hrubÿ parameter can be calculated by $K_H = (T_c - T_g)/(T_m - T_c)$, where T_c is the *onset of crystallization temperature*, T_g *the mean glass transition temperature,* and T_m the *melting point* (Kozmidis-Petrovic and Šesták, 2012). These parameters were calculated from the onset temperatures in the DSC data (**Figure 6**).

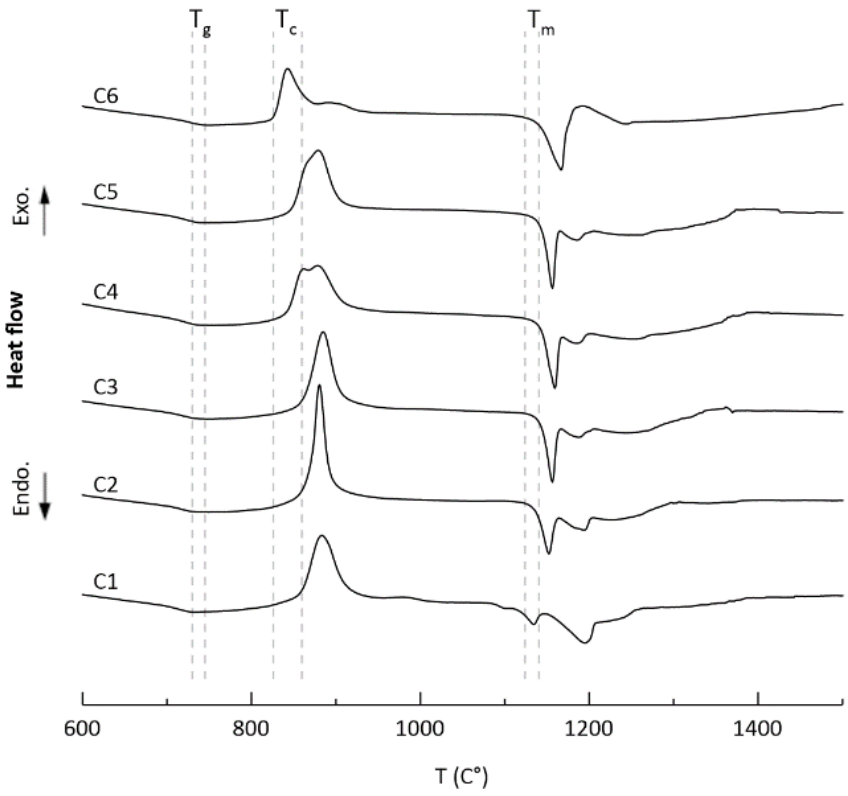

Figure 6: *Differential scanning calorimetry (DSC) data for the glass compositions with ranges indicated for the onset of crystallization T_c, mean glass transition temperature T_g, and melting point T_m.*

As aluminum content is increased in the glasses, T_c decreases and both T_g and T_m increase. Consequently the dividend decreases and denominator increases, decreasing the Hrubÿ parameter with increasing aluminum content (**Figure 7f**).

Since the Hrubÿ parameter is inversely related to the critical cooling rate, it can be used to explain the presence of phase separation in C6. Cabral *et al.* (1997) studied the relationship between the Hrubÿ parameter and the critical cooling rate of different silicate glasses, and found a K_H of 0.27 for Na-Ca-Si glasses corresponding to a critical cooling rate of 3-6 K/s, and that of 0.42 corresponding to 0.2-0.3 K/s. Since we used the same cooling procedure for all glasses, with an estimated cooling rate of 13.0 K/s, it can be seen that as aluminum content is increased the cooling rate gets closer to the critical cooling rate.

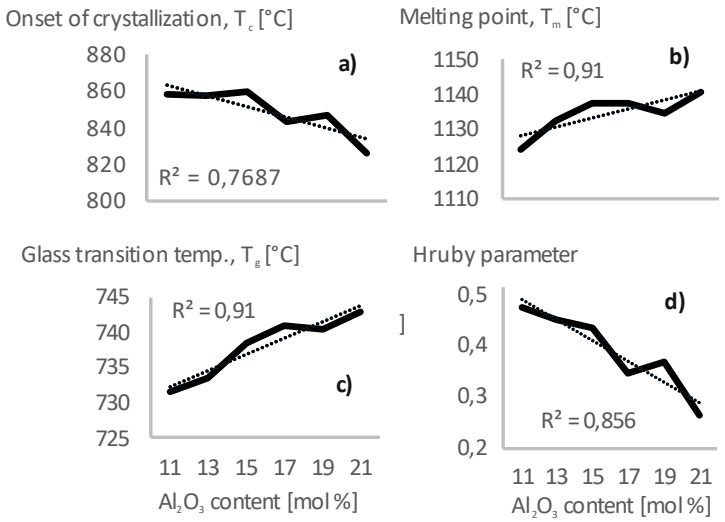

Figure 7: *Properties of the prepared glasses as a function of aluminum content. a) Onset of crystallization, T_c, b) melting point T_m, and c) mean glass transition temperature T_g, were used to calculate the Hrubÿ parameter shown in d).*

The relationship between glass cooling rate, nucleation and crystallization can be visualized using a time-temperature-transformation (TTT) diagram (**Figure 8**). Glass held at a temperature above the crystallization temperature will nucleate and after some time begin to crystallize (Liu and Zhang, 2015). Presumably, therefore, in C6 the cooling rate used was close enough to the critical cooling rate to initiate nucleation, but was still below the critical cooling rate to avoid crystallization. This type of nucleation without crystallization during cooling leads to glass-glass phase separation as seen in C6. This is also

consistent with previous results, as Moesgaard *et al.* (2007) found that similar stone wool compositions will first form phase separated glassy phases before crystallizing via homogenous nucleation.

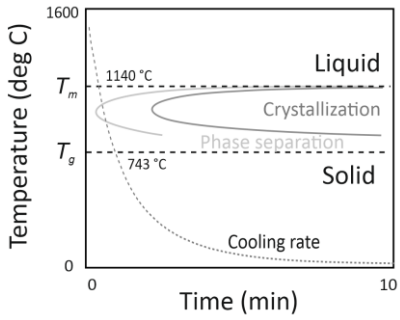

Figure 8: *A schematic time-temperature-transformation (TTT) diagram for C6 that at a certain cooling rate nucleation happens without crystallization in the glass. The actual measured cooling rate shown, along with T_m and T_g for C6.*

Therefore, the existence of phase separation in C6 (and not in C1) could be explained by a cooling rate that is close to the critical cooling rate that was found to increase with increasing Al_2O_3 as evidenced by a decreasing Hrubÿ parameter. The presence of phase separation in C6 can further explain the high leached fraction and rate of dissolution associated with this sample. These findings are consistent with the tendency for phase separation in basaltic stone wool glasses, and the increased reactivity associated with blast furnace slags.

In the presence of phase separation the reactivity of a glass becomes more complex as it can no longer be characterized by a single number, such as NBO/T. At the same time, the presence of phase separation enables decoupling of the glass reactivity from CaO content (and RM-CO_2 emissions).

CO_2 emissions: Chemical composition of the glass does not guarantee low total CO_2 emissions but can increase potential for it. Unlike high-calcium glasses and slags, the multicomponent composition used here does not necessitate the use of $CaCO_3$ as raw material. For example, a composition close to C6 could be achieved using RM-CO_2-free silicates: 50% anorthite ($CaAl_2Si_2O_8$), 30% olivine [$(Mg, Fe)_2SiO_4$], 15% wollastonite ($CaSiO_3$) and 5% Na_2O. **Figure 9** shows the glass compositions and the above-mentioned mix of silicates for comparison.

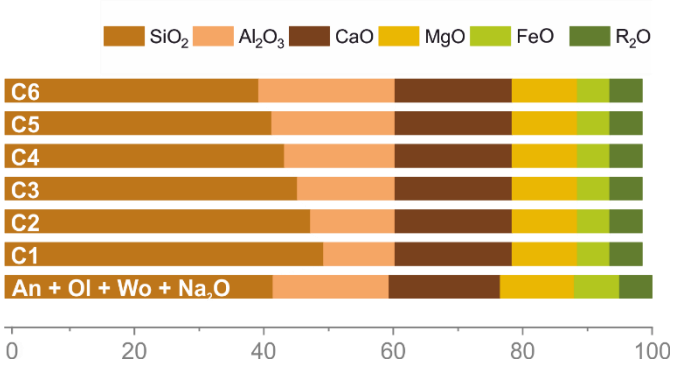

Figure 9: *Glass compositions compared to a silicate-based composition close to C6 with zero RM-CO_2 emissions [50% anorthite (An), 30% olivine (Ol), 15 % wollastonite (Wo), and 5% Na_2O]. R_2O contains K_2O and Na_2O, while TiO_2 is not shown.*

The compositions used are close to basaltic compositions. Basalt is the most common igneous rock, and because it is globally distributed and ubiquitous it is a potential feedstock for large volume applications. It is also being considered for large scale in-situ carbonation in carbon sequestration applications (Sanna et al., 2014).

Apart from the RM-CO_2 emissions, the other major source of carbon emissions in cement production is related to energy consumption. Portland cement is produced by calcining finely-ground raw materials at 1450 °C, resulting in a clinker that is ground to the required fineness. Assuming that the energy for milling are similar, differences in heating energy are the main differentiator. The average specific thermal energy consumption of Portland cement production is estimated to be 3.7 GJ/t clinker ("Cement Technology Roadmap 2009," 2010). Surprisingly, glass production can be performed with comparable energy; for glass production an efficient melting tank with maximum operating temperature of 1600 °C has a thermal energy consumption of ~3.8 GJ/t (Sardeshpande et al., 2007). Therefore, according to these rough estimates, the *energy-related* CO_2 emissions are comparable for glass production and Portland cement clinker production. The *raw material-related RM*-CO_2 can reach zero for the glass-based cement, given that the chemical composition of the produced glass allows for RM-CO_2-free silicate minerals to be used as the sole raw materials, while for Portland cement roughly 500 grams of CO_2 is liberated from the raw materials for every kilogram of cement produced (Gartner, 2004).

In alkali activated materials, there will be additional emissions related to the activator. In the best-case scenario, the activation can be done with Na_2CO_3, as is the case with blast furnace slag, in which case the activator-related emissions will be low as well. Na_2CO_3 is produced via chlor-alkali process, with the overall reaction:

$$2\ NaCl + CaCO_3 \rightarrow Na_2CO_3 + CaCl_2$$

One mole of $CaCl_2$ is produced for each mole of Na_2CO_3, so it is important that there are adequate markets for both chemicals. Fortunately, $CaCl_2$ is a common chemical which is used in large volumes in many applications, including fertilization, de-icing, dust control, oil well drilling, and food processing and therefore market can absorb large quantities of it. There are some CO_2 emissions associated with the chlor-alkali process as well. However, the CO_2 emissions are quite low at 0.4 % of the produced Na_2CO_3 by weight, and can therefore be neglected here (U.S. Environmental Protection Agency, 1992).

4. Conclusions

In this first attempt at silicate-mineral-based alkali-reactive glasses with zero RM-CO_2 emissions, we have studied the reactivity and the effect of aluminium content of basaltic glasses, inspired by commercial stone wool compositions. The glasses formed were found to be highly reactive, and the reactivity was associated with phase separation in the most aluminium-rich sample (22% Al_2O_3). The phase separation was introduced to the glass during cooling by using a cooling rate that was close to the critical cooling rate. The phase-separated glass consisted of silicon-rich and modifier-rich regions, with aluminium concentrated in the modifier-rich regions. The basalt glasses investigated have previously been found to nucleate and undergo glass-glass phase separation well before crystallization in temperatures below T_g, which is a requirement in forming the phase-separated glass.

5. Conflicts of interest

There are no conflicts to declare.

6. Acknowledgements

This work was supported by Academy of Finland (grant #292526), and an STSM Grant from COST Action CA15102.

7. References

Barati, M., Esfahani, S., Utigard, T.A., 2011. Energy recovery from high temperature slags. Energy 36, 5440–5449.

Cabral, A.A., Fredericci, C., Zanotto, E.D., 1997. A test of the Hruby parameter to estimate glass-forming ability. Journal of non-crystalline solids 219, 182–186.

Cement Technology Roadmap 2009 [WWW Document], 2010. URL https://www.iea.org/publications/freepublications/publication/Cement.pdf (accessed 8.25.15).

Cheng, A., Lin, W.-T., Huang, R., 2011. Application of rock wool waste in cement-based composites. Materials & Design 32, 636–642. https://doi.org/10.1016/j.matdes.2010.08.014

Devreux, F., Cailleteau, C., Barboux, P., 2010. Evidence for a threshold in the biosolubility of aluminosilicate vitreous fibers. Journal of materials science 45, 1154–1159.

Durdziński, P.T., Snellings, R., Dunant, C.F., Haha, M.B., Scrivener, K.L., 2015. Fly ash as an assemblage of model Ca–Mg–Na-aluminosilicate glasses. Cement and Concrete Research 78, Part B, 263–272. https://doi.org/10.1016/j.cemconres.2015.08.005

Gartner, E., 2004. Industrially interesting approaches to "low-CO2" cements. Cement and Concrete Research 34, 1489–1498. https://doi.org/10.1016/j.cemconres.2004.01.021

Greaves, G.N., Sen, S., 2007. Inorganic glasses, glass-forming liquids and amorphizing solids. Advances in Physics 56, 1–166.

Guldberg, M., Jensen, S.L., Knudsen, T., Steenberg, T., Kamstrup, O., 2002. High-Alumina Low-Silica HT Stone Wool Fibers: A Chemical Compositional Range with High Biosolubility. Regulatory Toxicology and Pharmacology 35, 217–226. https://doi.org/10.1006/rtph.2001.1523

Habert, G., Ouellet-Plamondon, C., 2016. Recent update on the environmental impact of geopolymers. RILEM technical Letters 1, 17–23.

Hamilton, J.P., Brantley, S.L., Pantano, C.G., Criscenti, L.J., Kubicki, J.D., 2001. Dissolution of nepheline, jadeite and albite glasses: toward better models for aluminosilicate dissolution. Geochimica et Cosmochimica Acta 65, 3683–3702. https://doi.org/10.1016/S0016-7037(01)00724-4

Henderson, G.S., 2005. The structure of silicate melts: a glass perspective. Can Mineral 43, 1921–1958. https://doi.org/10.2113/gscanmin.43.6.1921

Hill, R.G., Wilson, A.D., 1988. Some structural aspects of glasses used in ionomer cements. Glass technology 29, 150–158.

Intergovernmental Panel on Climate Change, Edenhofer, O. (Eds.), 2014. IPCC, 2014: Climate Change 2014: Mitigation of Climate Change. Contribution of Working Group III to the Fifth Assessment Report of the Intergovernmental Panel on Climate Change. Cambridge University Press, New York, NY.

Jantzen, C.M., Plodinec, M.J., 1984. Thermodynamic model of natural, medieval and nuclear waste glass durability. Journal of Non-Crystalline Solids 67, 207–223.

Juenger, M., Provis, J.L., Elsen, J., Matthes, W., Hooton, R.D., Duchesne, J., Courard, L., He, H., Michel, F., Snellings, R., Belie, N.D., 2012. Supplementary Cementitious Materials for Concrete: Characterization Needs. MRS Online Proceedings Library Archive 1488. https://doi.org/10.1557/opl.2012.1536

Karamanov, A., Pisciella, P., Cantalini, C., Pelino, M., 2000. Influence of Fe3+/Fe2+ Ratio on the Crystallization of Iron-Rich Glasses Made with Industrial Wastes. Journal of the American Ceramic Society 83, 3153–3157. https://doi.org/10.1111/j.1151-2916.2000.tb01697.x

Ke, X., Bernal, S.A., Provis, J.L., 2016. Controlling the reaction kinetics of sodium carbonate-activated slag cements using calcined layered double hydroxides. Cement and Concrete Research 81, 24–37. https://doi.org/10.1016/j.cemconres.2015.11.012

Kinnunen, P., Yliniemi, J., Talling, B., Illikainen, M., 2017. Rockwool waste in fly ash geopolymer composites. Journal of Material Cycles and Waste Management 19, 1220–1227. https://doi.org/10.1007/s10163-016-0514-z

Kozmidis-Petrovic, A., Šesták, J., 2012. Forty years of the Hrubý glass-forming coefficient via DTA when comparing other criteria in relation to the glass stability and vitrification ability. J Therm Anal Calorim 110, 997–1004. https://doi.org/10.1007/s10973-011-1926-6

Lee, S.K., Stebbins, J.F., 2000. The Structure of Aluminosilicate Glasses: High-Resolution ^{17}O and ^{27}Al MAS and 3QMAS NMR Study. The Journal of Physical Chemistry B 104, 4091–4100. https://doi.org/10.1021/jp994273w

Li, C., Sun, H., Li, L., 2010. A review: The comparison between alkali-activated slag (Si+Ca) and metakaolin (Si+Al) cements. Cement and Concrete Research 40, 1341–1349. https://doi.org/10.1016/j.cemconres.2010.03.020

Li, Y., Sun, H., Liu, X., Cui, Z., 2009. Effect of phase separation structure on cementitious reactivity of blast furnace slag. Sci. China Ser. E-Technol. Sci. 52, 2695–2699. https://doi.org/10.1007/s11431-008-0239-x

Lin, W.-T., Han, T.-Y., Huang, C.-C., Cheng, A., Huang, R., 2012. Using Rock Wool Wastes as Partial Replacement of Cement in Cement-Based Composites. Advanced Science Letters 8, 489–494. https://doi.org/10.1166/asl.2012.2334

Liu, W., Zhang, L., 2015. On the nano/micro-mechanics of metallic glass. Critical Reviews in Solid State and Materials Sciences 40, 137–163.
Malfait, W.J., Verel, R., Ardia, P., Sanchez-Valle, C., 2012. Aluminum coordination in rhyolite and andesite glasses and melts: Effect of temperature, pressure, composition and water content. Geochimica et Cosmochimica Acta 77, 11–26.
Merzbacher, C.I., Sherriff, B.L., Hartman, J.S., White, W.B., 1990. A high-resolution 29 Si and 27 Al NMR study of alkaline earth aluminosilicate glasses. Journal of Non-Crystalline Solids 124, 194–206.
Mills, K.C., Yuan, L., Jones, R.T., 2011. Estimating the physical properties of slags. Journal of the Southern African Institute of Mining and Metallurgy 111, 649–658.
Moesgaard, M., Herfort, D., Skibsted, J., Yue, Y., 2010. Calcium aluminosilicate glasses as supplementary cementitious materials. Glass Technology-European Journal of Glass Science and Technology Part A 51, 183–190.
Moesgaard, M., Herfort, D., Steenberg, M., Kirkegaard, L.F., Yue, Y., 2011. Physical performances of blended cements containing calcium aluminosilicate glass powder and limestone. Cement and Concrete Research 41, 359–364.
Moesgaard, M., Pedersen, H.D., Yue, Y.Z., Nielsen, E.R., 2007. Crystallization in stone wool fibres. Journal of Non-Crystalline Solids 353, 1101–1108. https://doi.org/10.1016/j.jnoncrysol.2006.12.026
Moesgaard, M., Poulsen, S.L., Herfort, D., Steenberg, M., Kirkegaard, L.F., Skibsted, J., Yue, Y., 2012. Hydration of Blended Portland Cements Containing Calcium-Aluminosilicate Glass Powder and Limestone. Journal of the American Ceramic Society 95, 403–409. https://doi.org/10.1111/j.1551-2916.2011.04902.x
Mysen, B.O., Richet, P., 2005. Silicate Glasses and Melts: Properties and Structure. Elsevier.
Mysen, B.O., Virgo, D., Seifert, F.A., 1985. Relationships between properties and structure of aluminosilicate melts. American Mineralogist 70, 88–105.
Mysen, B.O., Virgo, D., Seifert, F.A., 1982. The structure of silicate melts: Implications for chemical and physical properties of natural magma. Rev. Geophys. 20, 353–383. https://doi.org/10.1029/RG020i003p00353
Neuville, D.R., Cormier, L., Massiot, D., 2006. Al coordination and speciation in calcium aluminosilicate glasses: Effects of composition determined by 27 Al MQ-MAS NMR and Raman spectroscopy. Chemical geology 229, 173–185.
Newlands, K.C., Foss, M., Matchei, T., Skibsted, J., Macphee, D.E., 2017. Early stage dissolution characteristics of aluminosilicate glasses with blast furnace slag- and fly-ash-like compositions. J Am Ceram Soc 100, 1941–1955. https://doi.org/10.1111/jace.14716
Oey, T., Kumar, A., Pignatelli, I., Yu, Y., Neithalath, N., Bullard, J.W., Bauchy, M., Sant, G., 2017. Topological controls on the dissolution kinetics of glassy aluminosilicates. J Am Ceram Soc 100, 5521–5527. https://doi.org/10.1111/jace.15122
Panagiotopoulou, C., Kontori, E., Perraki, T., Kakali, G., 2007. Dissolution of aluminosilicate minerals and by-products in alkaline media. J Mater Sci 42, 2967–2973. https://doi.org/10.1007/s10853-006-0531-8
Perchuk, L.L., Kushiro, I., 2013. Physical Chemistry of Magmas. Springer Science & Business Media.
Perret, D., Crovisier, J.-L., Stille, P., Shields, G., Mäder, U., Advocat, T., Schenk, K., Chardonnens, M., 2003. Thermodynamic stability of waste glasses compared to leaching behaviour. Applied geochemistry 18, 1165–1184.
Qin, Y.L., Lv, X.W., Zhang, J., Hao, J.L., Bai, C.G., 2015. Determination of optimum blast furnace slag cooling rate for slag recycling in cement manufacture. Ironmaking & Steelmaking 42, 395–400. https://doi.org/10.1179/1743281214Y.0000000242
Sanna, A., Uibu, M., Caramanna, G., Kuusik, R., M. Maroto-Valer, M., 2014. A review of mineral carbonation technologies to sequester CO 2. Chemical Society Reviews 43, 8049–8080. https://doi.org/10.1039/C4CS00035H
Sardeshpande, V., Gaitonde, U.N., Banerjee, R., 2007. Model based energy benchmarking for glass furnace. Energy Conversion and Management 48, 2718–2738. https://doi.org/10.1016/j.enconman.2007.04.013
Schöler, A., Winnefeld, F., Haha, M.B., Lothenbach, B., 2017. The effect of glass composition on the reactivity of synthetic glasses. https://doi.org/10.1111/jace.14759
Scrivener, K.L., John, V.M., Gartner, E.M., 2016. Eco-efficient cements: Potential, economically viable solutions for a low CO2, cement based materials industry. United Nations Environment Program (UNEP), Paris.
Snellings, R., 2013. Solution-Controlled Dissolution of Supplementary Cementitious Material Glasses at pH 13: The Effect of Solution Composition on Glass Dissolution Rates. J. Am. Ceram. Soc. 96, 2467–2475. https://doi.org/10.1111/jace.12480
Tiwary, J.N., Sarkar, S., Mishra, B., Mohanty, U.K., 2013. Structural aspects of blast furnace slag.
U.S. Environmental Protection Agency, 1992. Background Report (AP-42) Chlor-alkali industry.
Waychunas, G.A., Brown, G.E., Ponader, C.W., Jackson, W.E., 1988. Evidence from X-ray absorption for network-forming Fe2+ in molten alkali silicates. Nature 332, 251–253. https://doi.org/10.1038/332251a0
Wolff-Boenisch, D., Gislason, S.R., Oelkers, E.H., Putnis, C.V., 2004. The dissolution rates of natural glasses as a function of their composition at pH 4 and 10.6, and temperatures from 25 to 74 C. Geochimica et Cosmochimica Acta 68, 4843–4858.
Yliniemi, J., Kinnunen, P., Karinkanta, P., Illikainen, M., 2016. Utilization of Mineral Wools as Alkali-Activated Material Precursor. Materials 9, 312.
Yue, Y., Von der Ohe, R., Jensen, S.L., 2004. Fictive temperature, cooling rate, and viscosity of glasses. The Journal of chemical physics 120, 8053–8059.

1